Jurnal Polimesin
Department of Mechanical Engineering
State Polytechnic of Lhokseumawe
http://e-jurnal.pnl.ac.id/polimesin
e-ISSN : 2549-1999 No. : 5 Month : October
p-ISSN : 1693-5462 Volume : 23 Year : 2025

Processing dates: received on 2025-08-16, reviewed on 2025-09-14, accepted on 2025-10-15 and online availability on 2025-10-31

An in-situ experimental and numerical evaluation of thermoelectric generators' performance utilizing diesel engine exhaust heat

Sugiyanto[1,2], Nyayu Aisyah[1,*], Yosephus Ardean Kurnianto Prayitno[1,2], Irfan Bahiuddin[1]

[1]Department of Mechanical Engineering, University of Gadjah Mada, Yogyakarta 55281, Indonesia
[2]Center for Energy Studies, University of Gadjah Mada, Yogyakarta 55281, Indonesia
*Corresponding Author: nyayuaisyah@ugm.ac.id

Abstract

Waste Heat Recovery (WHR) from heavy-duty diesel generators using Thermoelectric Generators (TEGs) offers a potential way to improve total system efficiency and reduce fuel consumption. This study combines experiments and numerical simulation to evaluate the performance of Hi-Z HZ 14 TEGs modules applied to a 6-cylinder, 60 kVA diesel generator. Experimentally, TEG modules were mounted equidistantly along the exhaust manifold, 40 cm from the engine, and tested at idle (750 rpm) with and without active air- side cooling. Hot- and cold- side temperatures, open- circuit Voltage (Voc), load power, and conversion efficiency were recorded. A matching TEG configuration was simulated under the same boundary conditions. As a result, active cooling increased the temperature differential and consistently improved power output and efficiency relative to natural convection. An efficiency of 2.1% was observed, in reasonable agreement with the simulation and consistent with typical TEGs performance under comparable operating conditions. Although this value confirms the feasibility of TEG integration in heavy-duty diesel exhaust systems, further improvements are possible through material selection, heat-sink optimization, and advanced cooling strategies.

Keywords:
Thermoelectric generator, waste heat recovery, active cooling, combined performance evaluation, heavy-duty diesel generator

1 Introduction

Heavy-duty diesel generators are extensively used in construction, mining, and industrial operations because of their reliability, exceptional longevity, and consistent high-power output under extreme operational conditions [1][2]. However, their energy conversion efficiency remains low, typically 25% to 30%. This means that a considerable fraction of fuel energy, roughly 35%, is exhausted as waste heat, dissipated without doing practical work [3].

Unutilized thermal energy not only directly translates into fuel economy losses but also enhances operational costs while increasing greenhouse emissions [4][5]. Capturing and reusing this waste heat presents a strategic opportunity to enhance fuel economy and system performance, while reducing emissions. Of the numerous Waste Heat Recovery (WHR) technologies studied, Thermoelectric Generators (TEGs) stand out due to the absence of moving parts, their solid-state operation, scalability, and ability to convert temperature differentials to electrical power via the Seebeck effect [6][7]. Reliability and low-maintenance needs make TEGs desirable for integration into diesel generator systems [8]. Unfortunately, the low efficiency of TEGs, as rapidly as they can convert heat to electricity, is detrimental to commercial TEGs modules, which only have a 5-10% efficiency [9][10]. Although the effectiveness of commercially available TEGs remains low compared to other WHR technologies, their solid-state, compact, and integrated characteristics render them desirable for practical use in diesel-powered power systems. With the imperative to maximize energy efficiency and reduce emissions in heavy-duty generators, incremental improvements enabled by TEG technology can have significant cumulative impacts. To improve the cold-side cooling of the TEGs modules, the thermal management of the module needs to be improved. This, in turn, will allow the module to maximize efficiency and power output.

The use of liquid cooling, finned heatsinks, and even phase change materials have all been explored towards TEGs performance enhancement [11][12][13]. Most of the focus has been on small-scale engines in a laboratory setting, which makes it hard to relate the findings to larger diesel generators. Moreover, the research on commercial TEGs modules and performance benchmarking in realistic heat exhaust scenarios is limited.

In our prior work, in situ, field- calibrated measurements are essential for capturing the actual phenomenological dynamics of operating systems. For instance, the multiple- current–voltage (MCV) measurement frameworks coupled with deep learning to visualize and estimate void fraction transitions under non- stationary two- phase flows can demonstrate that instrumentation designed around real operating conditions produces data with the fidelity needed for model training and validation, rather than relying solely on laboratory surrogates [14][15]. Building on this, the experiment- anchored Multiphysics simulations to interpret transient thermofluidic and phase- change phenomena illustrate how calibrated simulations generalize experimental insights beyond a single test point [16][17]. By analogy, TEGs evaluation on diesel exhaust requires both in- situ measurements (to capture the actual exhaust pulsations, thermal gradients, contact resistances, and on- engine boundary conditions) and validated simulations (to deconvolve heat- transfer pathways and predict performance across the operating envelope). This integrated perspective is largely missing from prior TEG studies on generator sets and motivates the present experimental–simulation assessment.

Accordingly, this study addresses the identified gap by presenting a combined in- situ experimental and numerical simulation framework for evaluating TEGs waste- heat recovery on a six- cylinder, 60 kVA diesel generator. The TEGs modules are evaluated under realistic exhaust pulsations while varying module type, placement along the manifold, engine speed, and the presence of active cooling. The experimentally acquired temperature, ΔT, Voc, I–V, power, and efficiency data are then used to calibrate and validate the simulation, enabling attribution of performance to specific thermal- resistance pathways and operating variables.

2 Research methodology

The study is conducted in two main stages: the experimental investigation and the numerical simulation. In the first stage, the performance of the Bi_2Te_3-based TEG module (model HZ-14HV, 60.01 mm × 60.01 mm) was investigated on a heavy-duty six-cylinder, 60 kVA diesel generator to evaluate power output at different temperatures on both hot and cold sides. Based on similar operating conditions, the second stage is performed to assess the detailed performance of TEGs.

2.1 Experimental investigation

2.1.1 Installation configuration

The experimental setup for evaluating the TEG module is shown in Fig. 1 and is implemented on the exhaust pipe of a heavy-duty diesel generator. The experimental procedure was designed by adapting approaches commonly reported from previous works on

exhaust heat recovery with thermoelectric generators. In particular, the setup aligned with the methodology of Imran et al., who mounted TEG modules directly on the muffler of a diesel engine, used K-type thermocouples to measure temperatures on the hot and cold sides, and recorded the multimeter's precision electrical output [18]. While no specific international standard exists for in-situ TEG testing on exhaust systems, the present work followed standardized measurement practices, including sensor calibration and uncertainty evaluation, to ensure data reliability. The TEG assembly is mounted directly onto the exhaust surface using a machined aluminum heat sink to improve thermal conduction to the hot side. K-type thermocouples are strategically positioned: one on the exhaust pipe surface beneath the TEG hot side, and another embedded within the heat sink fins on the cold side. In this experiment, two thermocouples are used to monitor the temperature gradient across the module. An additional set of thermocouples measures the inlet and outlet air temperatures on the cooling side. Electrical output from the TEG is recorded using a precision digital multimeter, ensuring accurate measurements of both open-circuit voltage and load current.

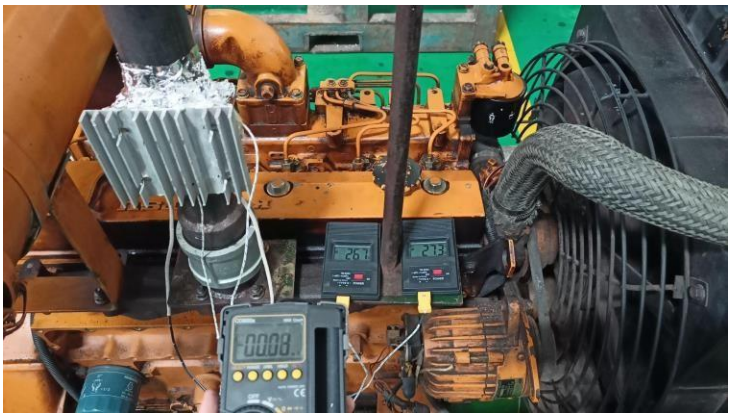

Fig. 1. Experimental setup

To enhance heat dissipation from the cold side during certain test runs, active forced-air cooling is introduced by channeling airflow from the generator alternator cooling outlet to the heat sink. This cooling source is selected because it utilizes existing airflow generated by the alternator fan, eliminating the need for additional energy input from external fans. The configuration enabled a direct comparison between natural convection cooling and active cooling conditions, allowing quantification of the performance improvement attributable to enhanced cold-side heat rejection.

2.1.2 Test procedures and calculation

The generator is set under an engine speed condition of 750 rpm. For each configuration (cooling mode on/off), data is recorded over a 10-minute steady-state period after thermal stabilization. Electrical power output (P) can be obtained by Eq. (1).

$$P = I^2R \tag{1}$$

where I is the measured current across the load resistor and R is the load resistor's resistance. While the conversion efficiency (η) was determined using Eq. (2).

$$\eta = \frac{T_h - T_c}{T_h} \times \frac{1 + ZT - 1}{1 + ZT - \frac{T_c}{T_h}} \tag{2}$$

with T_h is the hot-side temperature, T_c is the cold-side temperature, and ZT is the figure of merit.

2.2 Numerical simulation

2.2.1 TEGs 3D model and simulation

A 3D model of the cooling system was developed, incorporating the TEG modules, heatsink geometry, ducting, and mounting interfaces as seen in Fig. 2.

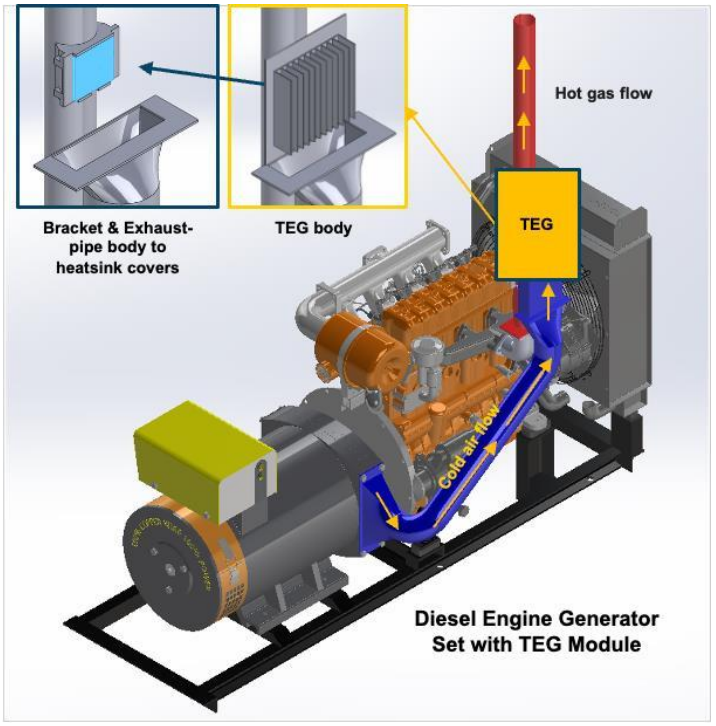

Fig. 2. TEG is integrated into the system

The numerical study was conducted using ANSYS Academic Research Mechanical and CFD, with Entitlement ID 1203476. In the numerical analysis, the model is set up as an internal-heat-transfer problem comprising two air streams: the diesel engine's hot exhaust gas from its muffler and the cold air flowing through the TEG module. These two models are separated by steel and aluminum solids representing the muffler and TEG materials. The geometric model was imported from CAD and partitioned into fluid and solid domains as boundary conditions with configurations of hot inlet, hot outlet, cold inlet, cold outlet, exhaust-pipe body, heatsink covers, bracket, and TEG body (see Fig. 2). Thus, the fluid-solid coupling at all wetted interfaces can be simulated.

To provide robust simulation results, a mesh-independent study with three grids, each evaluated and refined, was conducted, using a similar unstructured tetra/prism topology and a near-wall resolution suitable for the SST k−ω turbulence model. Here, mesh adequacy was assessed based on changes in outlet temperatures, TEG heat transfer, and pressure drops. Based on the study, convergence was accepted when the metrics varied by less than 1-2% for temperature and heat transfer rate, and by less than 3% for pressure drop. In addition, the mass imbalance was obtained to be below 0.5% with global energy balance error ≤ 1–2% for residual targets of 10^{-6} for energy and 10^{-3} for continuity/momentum/k/ω. Using integral monitors of flow, outlet temperature, and TEG heat flux, both numerical and physical parameters converged.

The ANSYS Fluent setup used a steady, pressure-based solver with the SST k–ω turbulence model. The energy equation was used with a conjugate calculation to simulate heat conduction through the steel pipe, aluminum heat sink components, and the TEG solid, accounting for convective heat transfer in both fluid domains. Gravity was neglected due to the minimum buoyancy as compared with the forced convection at the imposed throughflow velocities. The default compressible air configuration at low Mach numbers was maintained (constant properties, subsonic regime). Hybrid initialization was used from all fluid zones, and pseudo-transient under-relaxation (automatic timescale method) was employed to accelerate convergence of the steady RANS solution. Next, the material properties were set similar to the real experimental conditions. Each solid zone was assigned accordingly to ensure all fluid-solid interfaces were coupled with no prescribed wall temperature or heat flux. Hence, the interfacial heat flux is determined by the solution.

The experimental-numerical evaluation was conducted with two operating conditions of 750 rpm and 1500 rpm to represent the idle and load engine conditions, and the boundary conditions included:

a. As for the 750-rpm case, the hot-side velocity inlet was specified at U_h=28.7 m s−1 and T_h=91℃, while the cold-side velocity inlet was U_c=1.7 m s−1 and T_c=29.1℃.
b. As for the 1500 rpm case, the hot-side inlet was U_h=46.5 m s−1and T_h=127.3℃, and the cold-side inlet was U_c=3.0 m s−1with the same T_c=29.1℃.
c. At the inlet of both cases, turbulence quantities were prescribed using the Intensity and Viscosity Ratio option with a 5% turbulence intensity and a turbulent viscosity ratio of 10, consistent with internal duct flows of moderate roughness.
d. Both outlets (hot and cold) were defined as pressure outlets with zero-gauge pressure; backflow temperatures were set equal to the corresponding inlet temperatures to aid stability. All walls were no-slip, with thermal conditions "coupled" for the fluid–solid boundaries. External solid faces not in contact with fluid were treated as adiabatic unless explicitly part of a coupled interface.

The numerical simulations were conducted for a specific heatsink fin geometry, following the experimentally tested fin with a height of 90–150 mm and a specific ducting length, to assess their effect on cold-side temperature reduction. The primary performance metric was the ΔT across the TEG module, as an increase in ΔT directly correlates with higher electrical output.

2.2.2 Experimental-numerical evaluation

In the experimental study, η was obtained from a global calculation based on ΔT importance. For every configuration, the generator is operated at both 750 rpm and 1500 rpm. Data were averaged over the final 300 s of the 10- minute steady- state window to obtain ΔT. The measured exhaust- gas inlet temperature, ambient conditions, and cold- side temperature were observed during experiments. Temperature- dependent material properties are used, and the figure of merit ZT is evaluated at the mean module temperature. Model calibration is limited to a single baseline case (no- cooling) by adjusting the effective contact thermal resistance.

To provide a more detailed analysis, the numerical simulation is segmented. Referring to the z-axis of the TEGs 3D model with respect to the direction of the cooling air flow, the understanding of TEGs performance evaluation is enriched and comprehensively obtained.

3 Results and discussion

3.1 Experimental performance evaluation

The effect of the temperature difference (ΔT) between the hot and cold sides of the TEG modules on their performance has been described in Fig. 3 to Fig. 5. Evaluation was made on the three electrical performance metrics of interest: conversion efficiency, output current, and output voltage.

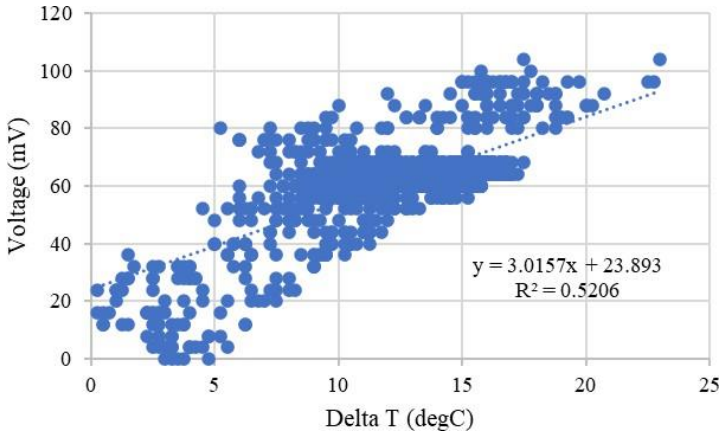

Fig. 3. Experimental correlation between temperature gradient and generated voltage in a heavy-duty diesel generator

Fig. 3 Shows the correlation between temperature gradient and generated voltage in a heavy-duty diesel generator: V = 3.0157ΔT + 23.893 (R^2 = 0.5206). This relationship suggests that the output voltage increases by approximately 3.02 mV per degree Celsius increase in ΔT and that there is a voltage offset of ~23.89 mV, which manifests at lower gradients and may be due to thermoelectric noise and a lack of uniform thermal distribution. The maximum output voltage is around 105 mV at a ΔT of approximately 22°C.

The relationship between output current and ΔT is given by I = 2.0371ΔT + 26.469 (R^2 = 0.5331), as seen in Fig. 4, which means that for every 1°C rise in ΔT, current increases by about 2.04 mA. The baseline current of about 26.47 mA is likely due to non-uniform heating and residual gradients. The current showed a peak of around 80 mA at a ΔT of around 22°C.

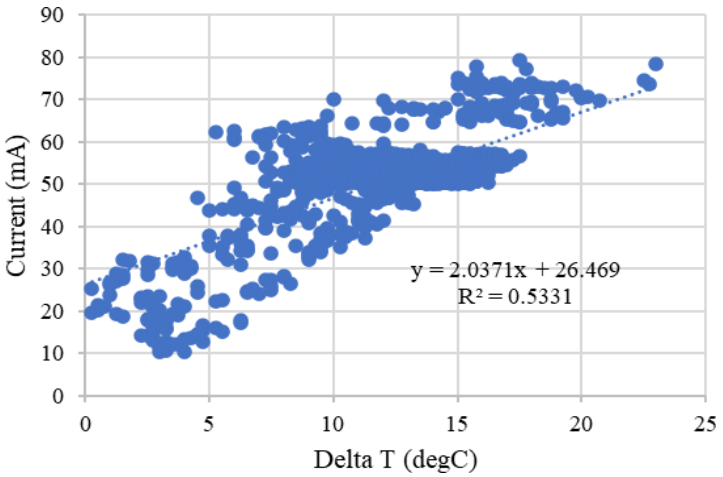

Fig. 4. Experimental correlation between temperature gradient and generated current in a heavy-duty diesel generator

The findings of this investigation, shown in Fig. 5, reveal a distinct positive correlation between the temperature difference (ΔT) across the TEG module and the generator's conversion efficiency. From the linear regression analysis, the following equation is obtained: $\eta = 0.1625\Delta T + 0.4341$, with a coefficient of determination R^2=0.5661. This indicates that, on average, a 1°C increase in ΔT leads to an efficiency increase of about 0.1625%, a statistically significant enhancement. The nonzero intercept (≈0.43%) observed at a temperature difference close to zero can be attributed to measurement and system noise, as well as unaccounted-for dynamic and static temperature differences in the system. This trend is consistent with previous results by Yin, T., et al. (2021), who found that efficiency increased steadily with ΔT in TEG modules. A similar proportional rise in η with ΔT confirms that the temperature gradient across the module primarily governs the thermoelectric conversion performance, consistent with the present experimental findings in the diesel-engine exhaust-based system [18].

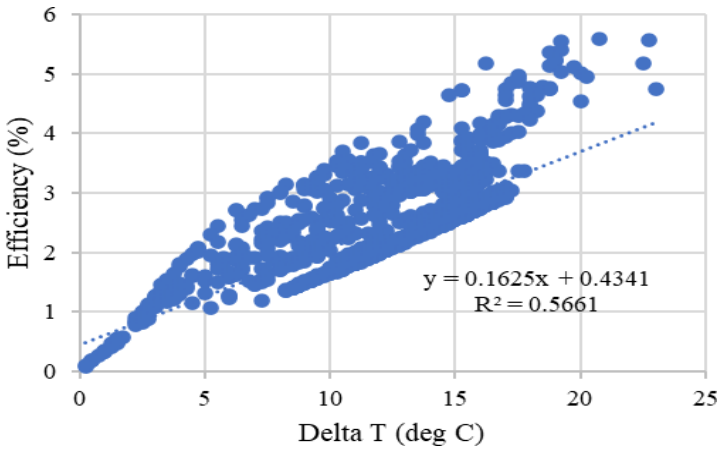

Fig. 5. Experimental correlation between temperature gradient and teg efficiency in a heavy-duty diesel generator

In this case, a moderate correlation with R^2 = 0.5661 is observed. This confirms the hypothesis that while ΔT remains a key performance factor for the thermal contact resistance [19], the degree of optimal load matching [20], the stability of the exhaust gas flow [21], and the effectiveness of the cooling mechanism on the cold side, which also significantly affects the thermoelectric generator's efficiency [22].

Measured efficiency peaked at around 5.5% with ΔT ≈ 22°C. This still falls short of the theoretical efficiency cap for Bi2Te3 modules operating under the same conditions, which is usually 7–8%. This gap indicates efficiency losses due to suboptimal thermal contacts or uneven thermal interfaces on the hot and cold sides. Improved forced-air cooling on the chilly side, as well as better thermal coupling on the exhaust surface, is likely to enhance ΔT, and thus, the efficiency is expected to be better [23].

For all three metrics evaluated, the R^2 values suggest a moderate degree of correlation, which means that while ΔT is the main, but not the only factor in determining TEGs performance, other factors also contribute, such as the degree of load matching, the line thermal contact resistance, the variation of exhaust gas flow rate, and the cooling efficacy on the cold side. These results strengthen the conclusion that there is a need to optimize thermal coupling on the hot side further and enhance heat rejection on the chilly side, primarily through active forced-air cooling. Hence, ΔT can be maximized, which in turn improves the overall electrical output and the efficiency of the system [24].

3.2 Experimental-numericalevaluation

Fig. 6 shows the steady- state temperature field around the exhaust manifold and TEGs module with a detailed hot- side block–module–cold- side sink and fin stack. The contours reveal a steep gradient concentrated across the module and mounting block, confirming that the dominant resistance lies in the hot- side contact and the TEGs body. The blue–green isotherms (333-364°C) within the fins indicate effective air- side heat removal. The warm "halo" in the pipe wall highlights lateral heat spreading in the manifold, which weakens with increasing distance from the module. This finding is consistent with an on- engine environment where conduction through the mounting block and the local convective film coefficient jointly set ΔT [25].

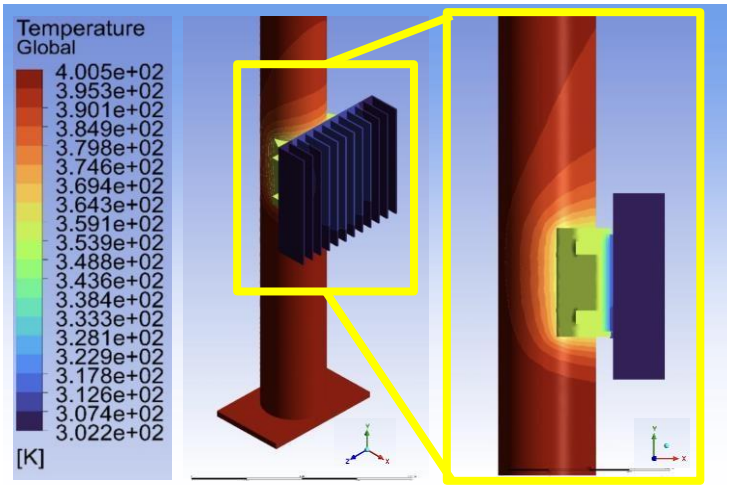

Fig. 6. TEGs modules temperature distribution for 1500 rpm case (peak temperature ≈ 400 K (≈ 127 °C) near the pipe–TEG contact with fins are ~333–364 K (60–91 °C))

Fig. 7 shows the comparison of Experimental (Exp) and numerical (Sim) efficiency calculated using Eq. (2). The Exp data were derived from the average of the selected experimental data, including the best ΔT and η, as well as the max, min, mean, and modus temperature of T_h / T . Since the Exp data were not a single data point, the standard deviation of η was calculated as 1.23, indicating that the range of η spans from the highest η = 3.47 to the lowest η = 0.67. On the other hand, the Sim data were numerically calculated as a single point from the global evaluation of ΔT across the whole simulation domain. The comparison gave an absolute error of 0.42. In addition, the numerical efficiency (2.24%) differs from the experimental mean (1.82–1.89%) by 0.35–0.42 percentage points, which are 0.28–0.34 σ, and falls within the experimental 95% confidence interval (0.60–3.18%). This indicates good agreement, with any residual offset attributable to on- engine boundary- condition variability rather than systematic model bias [26], [27].

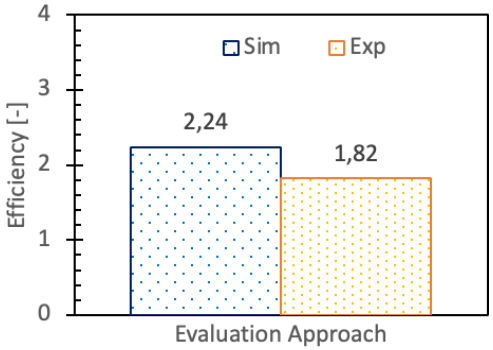

Fig. 7. Comparison of experimental and numerical efficiency

3.3 Segmented temperature-efficiency distribution

Fig. 8 couples the numerical temperature field around the TEGs module assembly with a three- segment analysis along the module height (A: lower, B: middle, C: upper). Segments A and C exhibit larger ΔT (~49.9 °C and 48.3 °C, respectively), whereas the middle segment B shows a reduced ΔT (~37.4 °C). This distribution is consistent with the underlying flow and heat-transfer field. On the cold (fin) side, the entrance and exit regions at the lower (A) and upper (C) ends experience more vigorous convection due to inlet impingement, outlet extraction, and edge effects around the fin tips. These mechanisms depress the local fin temperature, thereby increasing ΔT across the TEG at A and C. In contrast, at mid-height (B), the cold-side boundary layer is more fully developed, and the local heat-transfer coefficient is lower, leading to warmer fins and a diminished ΔT. On the hot side, the contact region between exhaust-pipe and TEG remains close to the imposed hot-inlet level (~400 K) with only mild axial decay, so the variation in ΔT is dominated by cold-side behavior. This spatial *T*pattern is

consistent with boundary-layer theory and recent measurements showing high local h near inlets/outlets, followed by decay in the thermally developed region, leading to warmer mid-span surfaces and smaller ΔT [28].

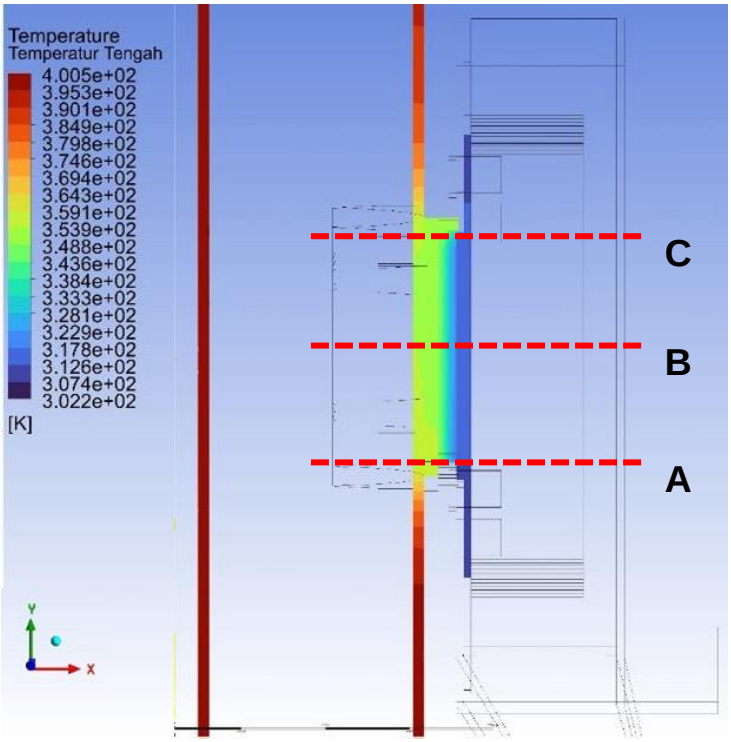

Fig. 8. Segmented temperature-efficiency distribution for 1500 rpm

As seen in Fig. 9, the variation of η between experimental and numerical simulation with respect to the three-segment provides a different trend. Thus, efficiency at the middle segment is 26% lower than at the lower segment in the experiment (2.17 vs. 2.94%) and 39% lower in the numerical result (1.76 vs. 2.89%), mirroring the 25% drop in ΔT from A to B (49.9 → 37.4 °C). Agreement is strong at A and C, with absolute differences of 0.05 and 0.08 percentage points, respectively. The most significant discrepancy occurs at B (0.40 percentage points), yet the model still captures the correct ranking (A ≈ C > B), indicating overall good predictive performance. The comparable pattern is found in the work by Doraghi et al. [29].

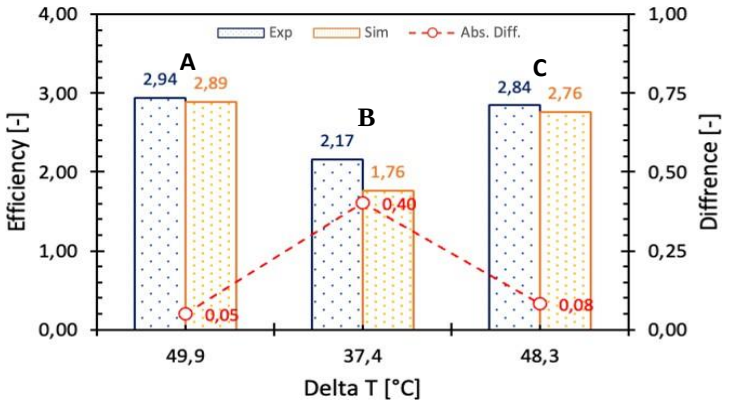

Fig. 9. Comparison of experimental and numerical efficiency

The spatial pattern is physically consistent with the temperature map. Near the lower and upper edges of the fin stack (A and C), enhanced mixing and edge- impingement promote greater cold- side heat removal (lower T_c), sustaining higher ΔT and η. Similar non-uniform convection was reported by Purohit et al. [30], where mid-span recirculation lowered heat transfer while edge impingement enhanced it. In contrast, the middle segment (B) experiences weaker local convection, likely due to recirculation/shadowing within the fin array and lateral heat spreading in the manifold, which elevates T_c and depresses ΔT. The larger model–experiment gap at B plausibly stems from idealized inlet flow profiles and simplified treatment of contact resistances, which under- resolve three- dimensional buoyancy and jet- interaction effects in the central region.

In practice, the segmented analysis shows that air- side maldistribution, rather than bulk property errors, limits performance uniformity. Design remedies suggested by the map include: (a) Fin re- spacing or a shallow shroud to equalize through- flow, as discussed by Zhang et al. [31] while designing a maldistribution-reduction manifold, (b) targeted flow guides to reduce mid- height recirculation, as conducted by Byun et al. [32] when directing the air in a radial heat sink, and (c) attention to hot- side/contact resistances that compound the mid- section penalty, these measures are expected to raise ΔT in the center segment and narrow the residual numerical–experimental gap.

4 Conclusions

This work presents an in-situ experimental and CFD-based numerical framework for evaluating TEGs performance on a six-cylinder, 60 kVA diesel generator at idle (750 rpm) and load (1500rpm). The main conclusions are as follows:

a. Numerical efficiency (2.24%) closely matches the experimental mean (1.82–1.89%), with an absolute difference of 0.35–0.42 percentage points and lies within the experimental 95% confidence interval (0.60–3.18%). This indicates good agreement and supports the use of the model for design and extrapolation. However, the overall efficiency remains lower than some cited studies because of the limited ΔT, contact thermal resistance, and cooling constraints.
b. Experimental regressions show that voltage, current, and efficiency increase with ΔT (e.g., $\eta = 0.1625\Delta T + 0.4341$, with R^2=0.5661), confirming ΔT as the primary determinant of TEG performance. Forced convection using alternator discharge air for increases ΔT, power and efficiency relative to natural convection, consistent with the temperature-field observation.
c. The reduced efficiency at mid-height (segment B) results from a thicker cold-side boundary layer, diminished local convection, and stronger lateral heat spreading, which together suppress the local ΔT. Conversely, the edge regions (segments A and C) benefit from entrance/exit acceleration and edge cooling at fin tips, producing higher convective coefficients, larger ΔT, and thus greater η. Under idle operation, the system attains a field-relevant average efficiency of ≈ 2%, establishing a clear baseline for subsequent design iterations.

These findings serve as both design guidelines and performance benchmarks for the integration of TEG-based waste heat recovery systems in large-scale diesel generator applications. Future research should look into the variation of operating conditions, TEGs specifications, its economic viability and cost analysis for industrial implementation.

Acknowledgements

The Academic Excellence Research Funding Program from Universitas Gadjah Mada 2025 supported this work. This study was conducted as part of an academia-industry collaboration between Universitas Gadjah Mada, Indonesia, and PT. United Tractors, Tbk, Indonesia.

References

[1] Z. Quan, L. Ge, Z. Wei, Y. W. Li, and L. Quan, "A survey of powertrain technologies for energy-efficient heavy-duty machinery," Proceedings of the IEEE, vol. 109, no. 3, pp. 279–308, 2021.

[2] A. Pronk, J. Coble, and P. A. Stewart, "Occupational exposure to diesel engine exhaust: a literature review," J Expo Sci Environ Epidemiol, vol. 19, no. 5, pp. 443–457, 2009.

[3] J. S. Jadhao and D. G. Thombare, “Review on exhaust gas heat recovery for IC engine,” International Journal of Engineeringa and Innovative Technology (IJEIT), vol. 2, no. 12, 2013.

[4] B. Duraivel et al., “A comprehensive review of Trinitor components: A sustainable waste heat recovery polygenerative system for diesel vehicles,” J Therm Anal Calorim, vol. 149, no. 5, pp. 1963–2006, 2024.

[5] J. G. Haidar and J. I. Ghojel, “Waste heat recovery from the exhaust of low-power diesel engine using thermoelectric generators,” in Proceedings ICT2001. 20 International Conference on Thermoelectrics (Cat. No. 01TH8589), IEEE, 2001, pp. 413–418.

[6] B. S. B. Singh, “Thermoelectric Generators: Design, Operation, and Applications,” in New Materials and Devices for Thermoelectric Power Generation, IntechOpen, 2023.

[7] M. d’Angelo, C. Galassi, and N. Lecis, “Thermoelectric materials and applications: a review,” Energies (Basel), vol. 16, no. 17, p. 6409, 2023.

[8] M. Comamala Laguna, “Development and characterization of thermoelectric generators for thermal energy recovery from reciprocating internal combustion engines,” 2019.

[9] R. Bjørk and K. K. Nielsen, “The performance of a combined solar photovoltaic (PV) and thermoelectric generator (TEG) system,” Solar Energy, vol. 120, pp. 187–194, 2015.

[10] N. Kanagaraj, “Photovoltaic and thermoelectric generator combined hybrid energy system with an enhanced maximum power point tracking technique for higher energy conversion efficiency,” Sustainability, vol. 13, no. 6, p. 3144, 2021.

[11] X. Liu, C.-F. Zhang, J.-G. Zhou, X. Xiong, and Y.-P. Wang, “Thermal performance of battery thermal management system using fins to enhance the combination of thermoelectric Cooler and phase change Material,” Appl Energy, vol. 322, p. 119503, 2022.

[12] S. H. Kim, C. S. Heu, J. Y. Mok, S.-W. Kang, and D. R. Kim, “Enhanced thermal performance of phase change material-integrated fin-type heat sinks for high power electronics cooling,” Int J Heat Mass Transf, vol. 184, p. 122257, 2022.

[13] H. Ruan et al., “Numerical investigation and comparative analysis of nanofluid cooling enhancement for TEG and TEC systems,” Case Studies in Thermal Engineering, vol. 27, p. 101331, 2021.

[14] K. Tanaka, Y. A. K. Prayitno, P. A. Sejati, D. Kawashima, and M. Takei, “Void fraction estimation in vertical gas-liquid flow by plural long short-term memory with sparse model implemented in multiple current-voltage system,” Multiphase Science and Technology, vol. 34, no. 2, 2022.

[15] D. Saito, Y. A. K. Prayitno, P. A. Sejati, S. Miwa, and M. Takei, “Spatio-temporal void fraction visualization in air-water two-phase flow regime transitions by combination of convolutional neural network and long short-term memory implemented into multiple current-voltage (MCV-CNN_LSTM),” Flow Measurement and Instrumentation, vol. 97, p. 102593, 2024.

[16] S. Segawa, P. A. Sejati, Y. A. K. Prayitno, N. Saito, and M. Takei, “Spatiotemporal distribution visualization of solid volume fraction during LiCl-KCl molten salt solidification by thermal-compensated electrical resistance tomography (tcERT),” Advanced Powder Technology, vol. 35, no. 12, p. 104723, 2024.

[17] A. A. Luthfie, S. Segawa, Y. A. K. Prayitno, N. Saito, and M. Takei, “Complex impedance transition of molten sodium chloride during crystallization process by transient enthalpy porosity-impedance (TEP-I) model compared with multi- layered impedance measurement,” Electrochim Acta, p. 146245, 2025.

[18] T. Yin, W.-T. Li, K. Li, and Z.-Z. He, “Multi-parameter optimization and uncertainty analysis of multi-stage thermoelectric generator with temperature-dependent materials,” Energy Reports, vol. 7, pp. 7212–7223, 2021.

[19] Y. Tian et al., “THERMAL CONTACT RESISTANCE MATCHING TO OPTIMIZE PERFORMANCE IN THERMOELECTRIC GENERATORS,” Journal of Enhanced Heat Transfer, vol. 27, no. 7, pp. 617–627, 2020, doi: 10.1615/JEnhHeatTransf.2020034270.

[20] J. Zhao, Z. Kuang, R. Long, Z. Liu, and W. Liu, “Impacts of thermal and electric contact resistance on the material design in segmented thermoelectric generators,” Energy Storage and Saving, vol. 3, no. 1, pp. 5–15, 2024, doi: 10.1016/j.enss.2023.12.001.

[21] F. Zhang, L. Cheng, M. Wu, X. Xu, P. Wang, and Z. Liu, “Performance analysis of two-stage thermoelectric generator model based on Latin hypercube sampling,” Energy Convers Manag, vol. 221, 2020, doi: 10.1016/j.enconman.2020.113159.

[22] Y. Cai, J. Xiao, W. Zhao, X. Tang, and Q. Zhang, “A general model for the electric power and energy efficiency of a solar thermoelectric generator,” in Journal of Electronic Materials, 2011, pp. 1238–1243. doi: 10.1007/s11664-011-1616-y.

[23] Z. Ma, X. Wang, and A. Yang, “Influence of temperature on characters of thermoelectric generators based on test bed,” J Nanomater, vol. 2014, 2014, doi: 10.1155/2014/719576.

[24] D. Luo, R. Wang, W. Yu, and W. Zhou, “A numerical study on the performance of a converging thermoelectric generator system used for waste heat recovery,” Appl Energy, vol. 270, 2020, doi: 10.1016/j.apenergy.2020.115181.

[25] W. Zhang and X. Su, “Effect of an internal thermal-conductive cylinder on the conjugate conduction-convection in an enclosure,” Numeri Heat Transf A Appl, vol. 80, no. 10, pp. 505–523, 2021, doi: 10.1080/10407782.2021.1959824.

[26] Q. Doraghi and H. Jouhara, “Thermoelectric generator efficiency: An experimental and computational approach to analysing thermoelectric generator performance,” Thermal Science and Engineering Progress, vol. 55, 2024, doi: 10.1016/j.tsep.2024.102884.

[27] E. Kanimba, M. Pearson, J. Sharp, D. Stokes, S. Priya, and Z. Tian, “A comprehensive model of a lead telluride thermoelectric generator,” Energy, vol. 142, pp. 813–821, 2018, doi: 10.1016/j.energy.2017.10.067.

[28] J. H. Lienhard, “Heat Transfer in Flat-Plate Boundary Layers: A Correlation for Laminar, Transitional, and Turbulent Flow,” J Heat Transfer, vol. 142, no. 6, Jun. 2020, doi: 10.1115/1.4046795.

[29] Q. Doraghi and H. Jouhara, “Thermoelectric generator efficiency: An experimental and computational approach to analysing thermoelectric generator performance,” Thermal Science and Engineering Progress, vol. 55, p. 102884, Oct. 2024, doi: 10.1016/j.tsep.2024.102884.

[30] M. N, S. Purohit, and K. V. Karanth, “Computational flow and heat transfer study on impingement cooling in a turbine blade leading edge using an innovative convergent nozzles,” Journal of the Brazilian Society of Mechanical Sciences and Engineering, vol. 45, no. 2, p. 86, Feb. 2023, doi: 10.1007/s40430-023-04020-4.

[31] M. Zhang, C.-M. Yang, K. Li, and K. Nawaz, “Reducing the Flow Maldistribution in Heat Exchangers through a Novel Polymer Manifold: Numerical Evaluation,” Energies (Basel), vol. 16, no. 20, p. 7120, Oct. 2023, doi: 10.3390/en16207120.

[32] S. Byun, S. Hyeon, and K.-S. Lee, “Guide Vane for Thermal Enhancement of a LED Heat Sink,” Energies (Basel), vol. 15, no. 7, p. 2488, Mar. 2022, doi: 10.3390/en15072488.